

## B-MESON DECAYS INTO FINAL STATES WITH A $\tau$ LEPTON

ABNER SOFFER

*School of Physics and Astronomy, Tel Aviv University  
 Tel Aviv, 69978, Israel  
 asoffer@tau.ac.il*

Received (Day Month Year)

Revised (Day Month Year)

Decays of  $B$  mesons into final states containing a  $\tau$  lepton are sensitive to new charged-current interactions that break lepton-flavor universality. These decays have been studied only at  $e^+e^-$  colliders, where the low-background environment and well-known initial state make it possible to observe small signals with undetectable neutrinos. In particular, the large data samples of the  $B$  factories and recent advances in techniques for full-event reconstruction have led to evidence for the decay  $B^+ \rightarrow \tau^+\nu_\tau$  and unambiguous observation of the decays  $B \rightarrow \bar{D}^{(*)}\tau^+\nu_\tau$ . These results exclude large regions of the parameter space for a variety of new-physics models. Furthermore, the branching fraction for  $B \rightarrow \bar{D}^{(*)}\tau^+\nu_\tau$  has been measured to be higher than the standard-model expectation by more than 3 standard deviations, making this an interesting topic for further research. This letter reviews the theoretical and experimental status of this topic, summarizing the results at this time and outlining the path for further improvements.

*Keywords:* B-meson decays;  $\tau$  lepton; B factory; new physics; two Higgs doublet model; charged Higgs; leptoquarks

PACS Nos.: 14.40.Nd, 14.60.Fg, 13.20.He, 13.20.-v

### 1. Introduction

The decays  $B \rightarrow \bar{D}^{(*)}\tau^+\nu_\tau$  and  $B^+ \rightarrow \tau^+\nu_\tau$  are well suited for searching for effects of new physics (NP) in charged-current interactions. In particular, the presence of third-generation fermions in both the initial and final-state leads to sensitivity to new particles that couple more strongly to heavy fermions, such as a charged Higgs.

The multiple neutrinos produced in these exclusive decays make it impossible to reconstruct the invariant mass of the  $B$  meson and use it for background rejection. Therefore, their study requires use of additional constraints related to the production of the  $B$  meson. Such constraints are available at  $B$  factories, which collide electrons and positrons at an average center-of-mass energy of  $\sqrt{s} \approx 10.58$  GeV, corresponding to the mass  $m_{\Upsilon(4S)}$  of the  $\Upsilon(4S)$  resonance. As a result, the  $B$  factories  $BABAR^{1,2}$  and Belle<sup>3</sup> have provided the only measurements of these decays.

The  $B$ -factory results include evidence for  $B^+ \rightarrow \tau^+\nu_\tau$  and more than 3.4-standard-deviation ( $\sigma$ ) difference between the  $B \rightarrow \bar{D}^{(*)}\tau^+\nu_\tau$  decay rates and the

expectation of the standard model (SM). Better understanding of this tension will come from improved measurements of the decay rates and the angular distributions at the current  $B$  factories. During the next decade, the Belle-II<sup>4</sup> experiment, which will have an integrated luminosity over 30 times greater than that of the combined *BABAR* and Belle datasets, will provide accurate measurements that should pinpoint possible NP contributions to these decays with great precision.

This paper is organized as follows. In Sec. 2 we discuss the theoretical background and predictions for measurements of  $B \rightarrow \bar{D}^{(*)}\tau^+\nu_\tau$  and  $B^+ \rightarrow \tau^+\nu_\tau$ . Sec. 3 outlines the experimental technique of full-event reconstruction, which is unique to the  $B$  factories and critical for enabling the study of these decays. We review the experimental results in Sec. 4, and discuss the implications for new physics in Sec. 5. Concluding remarks and the outlook for future measurements are given in Sec. 6.

## 2. Theory and Predictions

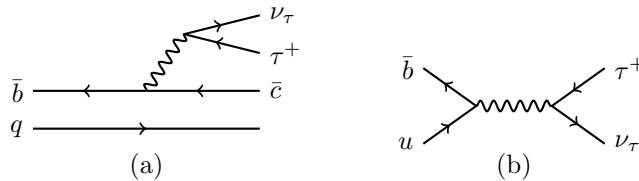


Fig. 1. Standard-model Feynman diagrams for  $B \rightarrow \bar{D}^{(*)}\tau^+\nu_\tau$  (a) and  $B^+ \rightarrow \tau^+\nu_\tau$  (b).

### 2.1. $B \rightarrow \bar{D}^{(*)}\tau^+\nu_\tau$ Theory

The SM Feynman diagram for  $B \rightarrow \bar{D}^{(*)}\tau^+\nu_\tau$  is shown in Fig. 1(a). The decay takes place via  $W$  emission, and in this respect is identical to  $B \rightarrow \bar{D}^{(*)}\ell^+\nu_\ell$  (where we use  $\ell$  to indicate an electron or muon). However,  $B \rightarrow \bar{D}^{(*)}\tau^+\nu_\tau$  is also sensitive to NP that preferentially impacts heavy fermions and thus escapes detection in  $B \rightarrow \bar{D}^{(*)}\ell^+\nu_\ell$ . A widely discussed example is mediation by a charged Higgs boson. The effective Hamiltonian that accounts for the SM plus new vector, scalar, and tensor interactions is<sup>5,6,7</sup>

$$\begin{aligned} \mathcal{H}_{\text{eff}} = & \frac{4G_F V_{cb}}{\sqrt{2}} [(1 + V_L) (\bar{c}\gamma_\mu P_L b) (\bar{\tau}\gamma^\mu P_L \nu_\tau) + V_R (\bar{c}\gamma_\mu P_R b) (\bar{\tau}\gamma^\mu P_L \nu_\tau) \\ & + S_L (\bar{c}P_L b) (\bar{\tau}P_L \nu_\tau) + S_R (\bar{c}P_R b) (\bar{\tau}P_L \nu_\tau) \\ & + T_L (\bar{c}\sigma^{\mu\nu} P_L b) (\bar{\tau}\sigma_{\mu\nu} P_L \nu_\tau)] + H.c., \end{aligned} \quad (1)$$

where  $G_F$  is the Fermi coupling constant,  $V_{cb}$  is the Cabibbo-Kobayashi-Maskawa (CKM) matrix elements<sup>8,9</sup>,  $\gamma_\mu$  are the Dirac matrices,  $\sigma_{\mu\nu} = i[\gamma_\mu, \gamma_\nu]/2$ ,  $P_{L,R} \equiv (1 \mp \gamma_5)/2$  are the left and right projection operators, and  $V_{L,R}$ ,  $S_{L,R}$ , and  $T_L$  are

complex Wilson coefficients that govern the NP contributions<sup>a</sup>. The SM corresponds to  $V_{L,R} = S_{L,R} = T_L = 0$ .

In what follows we take  $V_{L,R} = T_L = 0$  and focus on the scalar terms in Eq. (1) and on their implications for a charged Higgs boson. These terms describe the most general two-Higgs-doublet model, also known as type-III 2HDM. The more restricted type-II 2HDM, which is the Higgs sector of the minimal supersymmetric standard model, corresponds to  $S_L = 0, S_R = -m_b m_\tau \tan^2 \beta / m_{H^\pm}^2$ , where  $\tan^2 \beta$  is the ratio between the vacuum expectation values of the two Higgs doublets and  $m_{H^\pm}$  is the mass of the charged Higgs. The differential decay rate is then given by<sup>10</sup>

$$\frac{d\Gamma}{dq^2} = \frac{G_F^2 |V_{cb}|^2 p_{D^{(*)}}^* q^2}{96\pi^3 m_B^2} \left(1 - \frac{m_\tau^2}{q^2}\right)^2 \left[ (|H_+|^2 + |H_-|^2 + |H_0|^2) \left(1 + \frac{m_\tau^2}{2q^2}\right) + \frac{3}{2} \frac{m_\tau^2}{q^2} |H_s|^2 \right], \quad (2)$$

where  $p_{D^{(*)}}^*$  is the momentum of the  $D^{(*)}$  in the  $B$ -meson rest frame,  $q^2$  is the squared four momentum of the leptons, and  $H_x$  are  $q^2$ -dependent helicity amplitudes. The scalar terms in Eq. (1) affect only the  $H_s$  amplitude<sup>10,11,12</sup>:

$$H_s = H_s^{\text{SM}} \left[ 1 + (S_R \pm S_L) \frac{q^2}{m_\tau (m_b \mp m_c)} \right], \quad (3)$$

where the upper sign is for  $B \rightarrow \bar{D}\tau^+\nu_\tau$  and the lower is for  $B \rightarrow \bar{D}^*\tau^+\nu_\tau$ .

Hadronic uncertainties associated with the form factors that govern the helicity amplitudes are reduced, and the uncertainties due to constants such as  $V_{cb}$  and  $G_F$  are eliminated, when one studies the ratios of decay rates

$$R(D^{(*)}) \equiv \frac{\Gamma(B \rightarrow \bar{D}^{(*)}\tau^+\nu_\tau)}{\Gamma(B \rightarrow \bar{D}^{(*)}\ell^+\nu_\ell)}. \quad (4)$$

The numerator is obtained by integrating Eq. (2), and the denominator comes from the same expression with the replacement of  $m_\tau$  by  $m_\ell$ . The different  $q^2$  spectra of the two processes are accounted for in the helicity amplitudes. The SM values of these ratios have been calculated<sup>10,13,14</sup> using form factors obtained from  $B \rightarrow \bar{D}^*\ell^+\nu_\ell$  decays<sup>15</sup> and heavy quark effective theory<sup>16</sup>:

$$\begin{aligned} R_{\text{SM}}(D) &= 0.297 \pm 0.017, \\ R_{\text{SM}}(D^*) &= 0.252 \pm 0.03. \end{aligned} \quad (5)$$

An unquenched lattice-QCD calculation<sup>17</sup> yields for  $R_{\text{SM}}(D)$  a higher yet consistent value:

$$R_{\text{SM}}(D) = 0.316 \pm 0.012 \pm 0.07, \quad (6)$$

<sup>a</sup>Eq. (1) ignores the possibility of lepton-flavor violation in the leptonic terms<sup>7</sup>, since it is unobservable in this measurement.

where here and throughout the article, the first set of uncertainties is statistical and the second is systematic. A similar prediction,

$$R_{\text{SM}}(D) = 0.31 \pm 0.02, \quad (7)$$

has been obtained with only minimal reliance on theoretical input<sup>18</sup>. Eq. (5) and measurements<sup>19,20,21</sup> of  $\mathcal{B}(B \rightarrow \bar{D}^{(*)} \ell^+ \nu_\ell)$  yield the expected branching fractions<sup>10</sup>

$$\begin{aligned} \mathcal{B}(B^+ \rightarrow \bar{D}^0 \tau^+ \nu_\tau)_{\text{SM}} &= (0.66 \pm 0.05)\% \\ \mathcal{B}(B^0 \rightarrow D^- \tau^+ \nu_\tau)_{\text{SM}} &= (0.64 \pm 0.05)\% \\ \mathcal{B}(B^+ \rightarrow \bar{D}^{*0} \tau^+ \nu_\tau)_{\text{SM}} &= (1.43 \pm 0.05)\% \\ \mathcal{B}(B^0 \rightarrow D^{*-} \tau^+ \nu_\tau)_{\text{SM}} &= (1.29 \pm 0.06)\%. \end{aligned} \quad (8)$$

Eqs. (2) and (3) give the impact of the NP terms on the rate ratios,

$$\begin{aligned} R(D) &= R_{\text{SM}}(D) + A'_D \Re(S_R + S_L) + B'_D (S_R + S_L)^2, \\ R(D^*) &= R_{\text{SM}}(D^*) + A'_{D^*} \Re(S_R - S_L) + B'_{D^*} (S_R - S_L)^2, \end{aligned} \quad (9)$$

where  $A'_{D^{(*)}}$  and  $B'_{D^{(*)}}$  are coefficients that depend on the form factors and the quark masses. In a type-II 2HDM, this becomes

$$R(D^{(*)})_{\text{type II}} = R_{\text{SM}}(D^{(*)}) + A_{D^{(*)}} \frac{\tan^2 \beta}{m_{H^\pm}^2} + B_{D^{(*)}} \frac{\tan^4 \beta}{m_{H^\pm}^4}. \quad (10)$$

The coefficients in these expressions have been calculated<sup>14</sup> to be

$$\begin{aligned} A_D &= -3.25 \pm 0.32 \text{ GeV}^2, & A_{D^*} &= -0.230 \pm 0.029 \text{ GeV}^2, \\ B_D &= 16.9 \pm 2.0 \text{ GeV}^4, & B_{D^*} &= 0.643 \pm 0.085 \text{ GeV}^4, \\ A'_{D^*} &= -\frac{A_{D^*}}{m_\tau m_b}, & B'_{D^*} &= \frac{B_{D^*}}{m_\tau^2 m_b^2}. \end{aligned} \quad (11)$$

In addition to the total branching fraction and the  $q^2$  dependence of the decay rate, angular distributions can also be used to study NP contributions, as can CP-violating triple-product asymmetries that are non-zero when NP couplings are complex. The impact of NP contributions on the angular differential decay rates has been evaluated theoretically<sup>16,6,22</sup>, but has not yet been studied experimentally.

## 2.2. $B^+ \rightarrow \tau^+ \nu_\tau$ Theory

The SM Feynman diagram for  $B^+ \rightarrow \tau^+ \nu_\tau$  is shown in Fig. 1(b). Eq. (1) describes the effective Lagrangian for this process, following the quark replacement  $c \rightarrow u$  and accounting for a possible flavor dependence of the couplings. We again take  $V_{L,R} = T_L = 0$  to obtain the branching fraction prediction for the SM plus a new scalar interaction<sup>23</sup>,

$$\begin{aligned} \mathcal{B}(B^+ \rightarrow \tau^+ \nu_\tau) &= \frac{G_F^2 m_B m_\tau^2}{8\pi} \left(1 - \frac{m_\tau^2}{m_B^2}\right)^2 f_B^2 |V_{ub}|^2 \tau_B \\ &\times \left|1 + \frac{m_B^2}{m_\tau m_b} (S_R - S_L)\right|^2, \end{aligned} \quad (12)$$

where  $f_B = 189 \pm 4$  MeV is the  $B$ -meson decay constant<sup>24</sup>.

The largest uncertainty on the SM-predicted value of this branching fraction arises from the CKM element  $|V_{ub}|$ . The Particle Data Group<sup>25</sup> has calculated the world average value  $|V_{ub}| = (4.15 \pm 0.49) \times 10^{-3}$ , after scaling the measurement uncertainties by a factor of 2.6 to account for the roughly  $3\sigma$  difference<sup>25,26</sup> between the value obtained from the inclusive branching fraction  $\mathcal{B}(B \rightarrow X_u \ell^+ \nu_\ell)$  and the one from the exclusive branching fraction  $\mathcal{B}(B \rightarrow \pi \ell^+ \nu_\ell)$ . Eq. (12) then leads to the prediction

$$\mathcal{B}_{\text{SM}}(B^+ \rightarrow \tau^+ \nu_\tau) = (1.23 \pm 0.29) \times 10^{-4}; \quad (13)$$

The  $|V_{ub}|$  values obtained from global unitarity-triangle fits performed by the CKMfitter<sup>27</sup> and UTfit<sup>28</sup> collaborations favor the  $\mathcal{B}(B \rightarrow \pi \ell^+ \nu_\ell)$  results. The  $\mathcal{B}(B^+ \rightarrow \tau^+ \nu_\tau)$  values predicted by these fits are

$$\mathcal{B}_{\text{SM}}(B^+ \rightarrow \tau^+ \nu_\tau) = \begin{cases} 0.739_{-0.070}^{+0.090} \times 10^{-4} & \text{CKMfitter} \\ 0.81 \pm 0.07 \times 10^{-4} & \text{UTfit} \end{cases}. \quad (14)$$

The dependence on  $V_{ub}$  cancels in the ratio of branching fractions<sup>29,30,31,32</sup>

$$R' = \frac{\tau_{B^0}}{\tau_{B^+}} \frac{\mathcal{B}(B^+ \rightarrow \tau^+ \nu_\tau)}{\mathcal{B}(B^0 \rightarrow \pi^- \ell^+ \nu_\ell)}, \quad (15)$$

which is  $R' = 0.31 \pm 0.06$  in the SM<sup>33</sup>.

### 3. The Technique of Full-Event Reconstruction

A  $B$  factory is a high-luminosity  $e^+e^-$  collider with an average center-of-mass (CM) collision energy  $\sqrt{s}$  that equals the  $\Upsilon(4S)$  mass<sup>25</sup>,  $m_{\Upsilon(4S)} = 10.5794 \pm 0.0012$  GeV<sup>b</sup>. In what follows, we take all kinematic quantities in the average CM frame. The  $\Upsilon(4S)$  decays promptly to two  $B$  mesons, so that the  $B$  energy equals  $\sqrt{s}/2$  to within half the collision-energy spread, which is  $\sigma_{\sqrt{s}} \approx 5$  MeV at the current  $B$  factories<sup>2</sup>. The momenta of the two  $B$  mesons, which average 330 MeV, are equal to within  $\sigma_{\sqrt{s}}$  and opposite to within  $2^\circ$ .

These event characteristics are used to address the difficulties caused by undetectable neutrinos in rare  $B$ -meson decays. This is done by reconstructing not only the signal  $B$  decay of interest (labeled  $B_{\text{sig}}$ ), but also the other  $B$  meson in the event, known as the tag  $B$  (labeled  $B_{\text{tag}}$ ). In such full-event reconstruction, it is typically required that all charged-particle tracks be assigned to one of the two  $B$  candidates. Furthermore, the energy  $E_{\text{extra}}$  of unassigned calorimeter clusters or photon candidates is required to be low, typically around 1 GeV. This requirement reflects the fact that such ‘‘extra’’ energy arises not only from missing particles in background events, but also from calorimeter noise, previous events, and scattered

<sup>b</sup>We ignore the  $\mathcal{O}(\text{MeV})$  impact of initial-state radiation, which is anyway calibrated out in the measurement of  $\sqrt{s}$ .

particles from the interaction of hadrons with the calorimeter material in signal events.

By attempting to account for the origin of all particles in the event, full-event reconstruction reduces the rate of the combinatorial background, which arises from random combinations of particles that happen to satisfy the selection criteria. Furthermore, if the tag  $B$  is fully and correctly reconstructed in a hadronic final state, the kinematic constraints described above yield a measurement of the 4-momentum of the missing neutrinos, further aiding with signal identification and enabling the calculation of quantities in the signal- $B$  rest frame.

The disadvantage of full-event reconstruction is the low efficiency for reconstructing the large number of particles produced in a typical tag- $B$  decay<sup>34</sup>. Tag- $B$  final states with a high multiplicity of charged tracks and  $\pi^0$  mesons tend to also have low purity, defined as the fraction of correctly reconstructed decays among all selected  $B_{\text{tag}}$  candidates, due to the high combinatorial background. Nevertheless, the large datasets of *BABAR* and *Belle* and increasing sophistication in the application of  $B_{\text{tag}}$ -reconstruction techniques have made this technique an indispensable tool for the study of rare  $B$  decays and decays with multiple neutrinos.

Tag- $B$  reconstruction is performed by one of three techniques: hadronic tagging, semileptonic tagging, or inclusive tagging, depending on the  $B_{\text{tag}}$  final state and reconstruction method. The methods are generally complementary, with each having different advantages, disadvantages, and relative importance that depends, among other factors, on the signal- $B$  decay of interest. The details of each of these techniques are described in the following subsections.

### 3.1. Hadronic Tagging

In hadronic tagging, the tag  $B$  is fully reconstructed from its decay into a hadronic final state. Use of this technique was first reported by the ARGUS collaboration<sup>35</sup>. Since hadronic tagging provides the 4-momentum  $p_{\text{tag}}^\mu$  of the tag  $B$ , one can calculate the four-momentum of the undetectable neutrinos and their invariant mass, known as the missing mass:

$$\begin{aligned} p_{\text{miss}}^\mu &= \langle p_{e^+e^-}^\mu \rangle - p_{\text{tag}}^\mu - p_Y^\mu, \\ m_{\text{miss}}^2 &= p_{\text{miss}}^2, \end{aligned} \tag{16}$$

where  $Y$  denotes the visible particles in the final state of the signal decay and  $\langle p_{e^+e^-}^\mu \rangle$  is the average  $e^+e^-$  four-momentum, which is measured from the calibrated accelerator-beam parameters. The missing mass is useful for signal-background separation. Furthermore, the well-defined rest frame of the signal  $B$  allows calculation of  $q^2$  and  $p_{D^{(*)}}^*$  of Eq.(2), and additional variables that can be used for background suppression.

The tag  $B$  is reconstructed from decays that proceed via  $b \rightarrow c\bar{u}d$  or  $b \rightarrow c\bar{c}s$  transitions, which have the largest branching fractions due to their large CKM matrix elements. In most  $B$  decays, the charm quarks hadronize into a charmed

or charmonium meson. This is utilized for combinatoric-background reduction by reconstructing a  $D^{(*)+}$ ,  $D^{(*)0}$ ,  $D_s^{(*)-}$ , or  $J/\psi$  candidate, which is selected based on an invariant-mass criterion.

The kinematic characteristics of  $\Upsilon(4S) \rightarrow B\bar{B}$  events are brought into play by the use of two standard variables,

$$\Delta E = E_{\text{tag}} - \sqrt{s}/2, \quad m_{\text{ES}} = \sqrt{s/4 - p_{\text{tag}}^2}, \quad (17)$$

where  $E_{\text{tag}}$  and  $p_{\text{tag}}$  are, respectively, the reconstructed energy and momentum of the  $B_{\text{tag}}$  candidate. The expression for  $m_{\text{ES}}$  is essentially the  $B_{\text{tag}}$  invariant mass, with  $E_{\text{tag}}$  replaced by  $\sqrt{s}/2$ , which is much better known and measured independently of  $p_{\text{tag}}$ . For correctly reconstructed  $B_{\text{tag}}$  candidates,  $\Delta E$  and  $m_{\text{ES}}$  have nearly normal distributions that peak at 0 and  $m_B$ , with typical widths of 10 – 35 MeV and  $\sigma_{\sqrt{s}}/2$ , respectively. The typical background distribution under the signal peak is approximately linear in  $\Delta E$  and rapidly falling in  $m_{\text{ES}}$  with the diminishing phase space. Basic  $B_{\text{tag}}$  selection is accomplished by requiring  $\Delta E$  and  $m_{\text{ES}}$  to be within mode-dependent distances of their peak values.

In order to maximize efficiency and purity, final states with low particle multiplicity are preferred. However, the small total branching fraction of such decays necessitates use of higher-multiplicity decays as well. The number of  $B_{\text{tag}}$  reconstruction modes and the ways these modes are selected and handled have evolved over time. In the most recent hadronic-tagging analyses, *BABAR* and *Belle* reconstructed well over 1000  $B_{\text{tag}}$  modes, leading to approximately a four-fold increase in the effective  $B_{\text{tag}}$  efficiency relative to the earliest  $B$ -factory hadronic-tagging analysis<sup>36</sup>. This necessarily introduced many low-purity  $B_{\text{tag}}$  decays, requiring removal of as many incorrectly reconstructed  $B_{\text{tag}}$  candidates as possible while still maintaining high  $B_{\text{tag}}$ -reconstruction efficiency. The two collaborations developed different approaches for carrying this out.

The approach taken by *BABAR* was to simply remove the lowest-purity  $B_{\text{tag}}$  modes, where the purity of each mode was determined in a  $B_{\text{sig}}$ -decay-specific way from simulated events containing a true  $B_{\text{sig}}$  decay and a generic  $B_{\text{tag}}$  decay. This took advantage of the dependence of the purity on  $B_{\text{sig}}$ -specific factors, such as final-state multiplicity.

*Belle* considered the  $B_{\text{tag}}$  decay separately from the signal- $B$  decay, but applied a more sophisticated method of using  $B_{\text{tag}}$  information to obtain high purity and efficiency<sup>37</sup>. Tag- $B$  reconstruction was divided into four stages: (1) tracks, photons,  $K_S^0$ , and  $\pi^0$  candidates; (2) charmed-meson candidates; (3) excited charmed-meson candidates; and (4)  $B$  candidates. At each stage, neural-network algorithms were used to determine the probability that the  $B_{\text{tag}}$  components were correctly reconstructed, using input variables relevant for that stage. The product of the neural-network outputs of each stage was also used as an input variable for the subsequent stage. The output of the final neural-network was used, along with  $m_{\text{ES}}$  and  $\Delta E$ , for final  $B_{\text{tag}}$ -candidate selection<sup>38</sup>.

It is interesting to consider the possibility of further improvements in the purity

and efficiency of hadronic tagging. The *BABAR* method is better at exploiting the signal- $B$  decay, and the Belle method makes better use of information within the tag- $B$  decay. Combining the two approaches by executing the Belle method for each signal- $B$  mode separately may lead to further improvements.

### 3.2. Semileptonic Tagging

In semileptonic tagging, the tag  $B$  is reconstructed in the four semileptonic final states  $D^{(*)}\ell^-\nu_\ell$ , which make up  $(7.92\pm 0.17)\%$  and  $(7.11\pm 0.22)\%$  of the  $B^-$  and  $\bar{B}^0$  branching fractions, respectively<sup>25</sup>. So far, only the most favorable charmed-meson final states  $D^0 \rightarrow K^-\pi^+$ ,  $K^-\pi^+\pi^0$ ,  $K^-\pi^+\pi^-\pi^+$ ,  $K_S^0\pi^+\pi^-$ , and  $D^+ \rightarrow K^-\pi^+\pi^+$ ,  $K_S^0\pi^+$  have been used. The  $D^*$  decays have been  $D^{*+} \rightarrow D^0\pi^+$ ,  $D^{*+} \rightarrow D^+\pi^0$ ,  $D^{*0} \rightarrow D^0\pi^0$ , and  $D^{*0} \rightarrow D^0\gamma$ . In some cases<sup>39</sup>, there was no attempt to reconstruct the soft  $\pi^0$  or photon from the  $D^{*0}$  decay, in order to increase efficiency and also accept  $D^{*0} \rightarrow D^0\pi^0$  decays, at the cost of increased background.

Although the  $B_{\text{tag}}$  is not fully reconstructed, four-momentum conservation in its decay and the fact that its CM-frame 4-momentum is known yield the CM-frame angle between the momentum vector of the  $B_{\text{tag}}$  and that of the  $D^{(*)}\ell$  system,

$$\cos\theta_{B-D^{(*)}\ell} = \frac{E_{D^{(*)}\ell}\sqrt{s} - m_B^2 - m_{D^{(*)}\ell}^2}{2p_{D^{(*)}\ell}\sqrt{s/4 - m_B^2}}, \quad (18)$$

where  $E_{D^{(*)}\ell}$ ,  $m_{D^{(*)}\ell}$ , and  $p_{D^{(*)}\ell}$  are, respectively, the energy, invariant mass, and 3-momentum of the  $D^{(*)}\ell$  system. Tag- $B$  candidates are required to have  $\cos\theta_{B-D^{(*)}\ell}$  in a range somewhat larger than  $[-1, 1]$ , to allow for detector resolution and for the loss of a soft pion or final-state-radiation photons from an otherwise correctly reconstructed  $B_{\text{tag}}$  candidate. Background candidates may have  $\cos\theta_{B-D^{(*)}\ell}$  values well beyond the selection range.

### 3.3. Inclusive Tagging

In the inclusive-tagging method, one reconstructs the signal- $B$  candidate and then attempts to reconstructs the  $B_{\text{tag}}$  from all remaining tracks and photon candidates, while making no attempt to break the  $B_{\text{tag}}$  decay down according to known decay channels of the  $B$  meson. In further contrast to the hadronic-tagging method, only loose requirements on  $m_{\text{ES}}$  and  $\Delta E$  are applied, to allow for some lost particles, in particular  $K_L^0$  mesons, which are produced copiously in charm and bottom decays. All this makes inclusive tagging simpler and more efficient than hadronic tagging, while providing less background rejection. This technique was first used by the CLEO collaboration in the measurements of the  $B^0 \rightarrow \pi^-\ell^+\nu_\ell$  and  $B^0 \rightarrow \rho^-\ell^+\nu_\ell$  branching fractions<sup>40</sup>.

## 4. Experimental Results

We describe the results for  $B \rightarrow \bar{D}^{(*)}\tau^+\nu_\tau$  in Sec. 4.1, and those for  $B^+ \rightarrow \tau^+\nu_\tau$  in Sec. 4.2. The discussion focuses on the latest and most precise measurements,



summarizing older results briefly.

In addition to the full-event-reconstruction variables introduced in Sec. 3, each data analysis used requirements on various kinematic variables to suppress the background. Some of these variables quantified the difference between the isotropic distribution of particle momenta in  $\Upsilon(4S) \rightarrow B\bar{B}$  events and the jet-like structure of “continuum”  $e^+e^- \rightarrow q\bar{q}$  events, where  $q$  represents a  $u$ ,  $d$ ,  $s$ , or  $c$  quark. The other variables were analysis-specific, and were related to the degree of missing energy and momentum in the multi-neutrino signals, angular correlations between particle momenta, or invariant masses of intermediate resonances. The description here glosses over such details, focusing on the main measurement techniques and results.

#### 4.1. $B \rightarrow \bar{D}^{(*)}\tau^+\nu_\tau$ Results

We describe here the four *BABAR* and Belle journal publications on  $B \rightarrow \bar{D}^{(*)}\tau^+\nu_\tau$ , as well as a preliminary Belle result that has been used in a combination of the different measurements, which is presented in Sec.4.1.4. Physics interpretations of the results are discussed in Sec. 5.

##### 4.1.1. Belle Inclusive-Tagging Measurement

Belle made the first observation of a  $B \rightarrow \bar{D}^{(*)}\tau^+\nu_\tau$  decay in 2007, using a data sample of  $535 \times 10^6$   $B\bar{B}$  pairs and the inclusive-tagging method<sup>41</sup>. The signal  $B$  was reconstructed in the decay  $B^0 \rightarrow D^{*-}\tau^+\nu_\tau$ , taking advantage of the efficient background suppression provided by  $D^{*-} \rightarrow \bar{D}^0\pi^-$  reconstruction. The  $\bar{D}^0$  was reconstructed only in the channels  $\bar{D}^0 \rightarrow K^+\pi^-$  and  $\bar{D}^0 \rightarrow K^+\pi^-\pi^0$ , and the  $\tau^+$  was reconstructed in  $\tau^+ \rightarrow e^+\nu_e\bar{\nu}_\tau$  and  $\tau^+ \rightarrow \pi^+\bar{\nu}_\tau$ , the latter channel being also sensitive to  $\tau^+ \rightarrow \rho^+\bar{\nu}_\tau$ .

Peaking background, defined to be non-signal events with a peaking  $m_{\text{ES}}$  distribution and arising mostly from  $B^0 \rightarrow D^{*-}e^+\nu_e$ , was determined from simulation to constitute about 6 events. The signal and combinatorial-background yields were determined with a fit to the  $m_{\text{ES}}$  distribution. The signal yield was  $60^{+12}_{-11}$  events, with a significance<sup>c</sup> of  $5.2\sigma$ . The branching fraction was measured to be

$$\mathcal{B}(B^0 \rightarrow D^{*-}\tau^+\nu_\tau) = (2.02^{+0.40}_{-0.37} \pm 0.37) \%. \quad (19)$$

The  $m_{\text{ES}}$  distribution and the overlaid fit function are shown in Fig. 2(a).

In 2010, Belle reported a study of  $B^+ \rightarrow \bar{D}^{*0}\tau^+\nu_\tau$  and  $B^+ \rightarrow \bar{D}^0\tau^+\nu_\tau$  with the same analysis technique and a larger data sample of  $657 \times 10^6$   $B\bar{B}$  pairs<sup>42</sup>. In addition to the signal decay modes used for the 2007 analysis<sup>41</sup>, the decays

<sup>c</sup>All quoted signal significances account for the relevant systematic uncertainties.

<sup>d</sup>Fig. 2(a) is reprinted with permission from A. Matyja *et al.*, Phys. Rev. Lett. **99**, 191807 (2007). Copyright (2007) by the American Physical Society. Figs. 2(b-e) are reprinted with permission from A. Bozek *et al.*, Phys. Rev. Lett. **99**, 191807 (2007). Copyright (2010) by the American Physical Society.

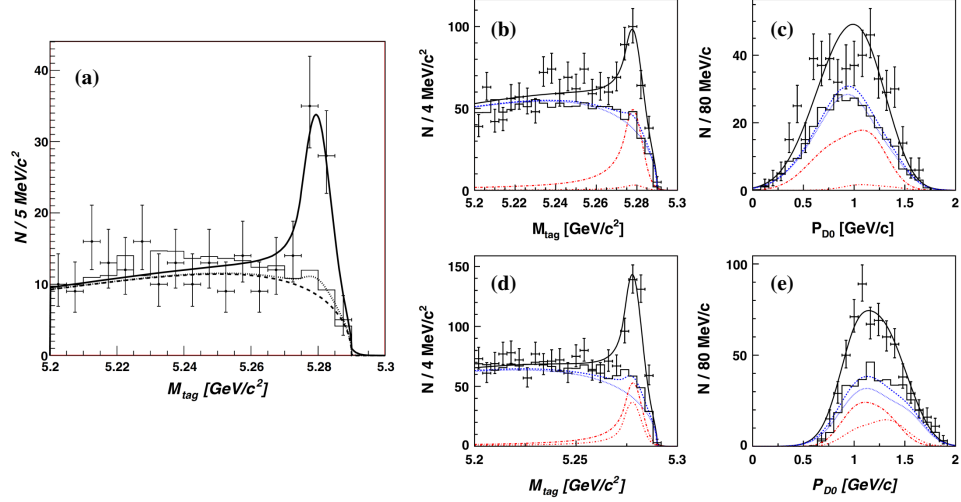


Fig. 2. The  $m_{\text{ES}}$  (labeled  $M_{\text{tag}}$ ) distribution of  $B^0 \rightarrow D^{*-}\tau^+\nu_\tau$  candidates at Belle<sup>41</sup> (a). The histogram shows the total expected background, and the dashed, dotted, and solid curves are the contributions to the fit from the combinatorial background, total background, and background plus signal, respectively. The  $m_{\text{ES}}$  (b) and  $D^0$  momentum (c) distributions of  $B^+ \rightarrow \bar{D}^{*0}\tau^+\nu_\tau$  candidates and (d,e)  $B^+ \rightarrow \bar{D}^0\tau^+\nu_\tau$  candidates at Belle<sup>42</sup>. The solid curve shows the total fit function, and the other curves show the fit contributions of the combinatorial background, total background, and  $B^+ \rightarrow \bar{D}^{*0}\tau^+\nu_\tau$  and  $B^+ \rightarrow \bar{D}^0\tau^+\nu_\tau$  signals. <sup>d</sup>

$\bar{D}^{*0} \rightarrow \bar{D}^0\pi^0$ ,  $\bar{D}^{*0} \rightarrow \bar{D}^0\gamma$ , and  $\tau^+ \rightarrow \mu^+\nu_\mu\bar{\nu}_\tau$  were used. Fits to the kinematic-variable distributions of a data sample selected with signal-rejection requirements were used to determine the relative contributions of different background sources. The signal and combinatorial-background yields were obtained from a fit to  $m_{\text{ES}}$  and the  $D^0$  momentum in the CM frame. The signal yields for  $B^+ \rightarrow \bar{D}^{*0}\tau^+\nu_\tau$  and  $B^+ \rightarrow \bar{D}^0\tau^+\nu_\tau$  were  $446^{+58}_{-56}$  and  $146^{+42}_{-41}$  events, respectively, with branching fractions of

$$\begin{aligned} \mathcal{B}(B^+ \rightarrow \bar{D}^{*0}\tau^+\nu_\tau) &= (2.12^{+0.28}_{-0.27} \pm 0.29) \% \\ \mathcal{B}(B^+ \rightarrow \bar{D}^0\tau^+\nu_\tau) &= (0.77 \pm 0.22 \pm 0.12) \% \end{aligned} \quad (20)$$

The decay  $B^+ \rightarrow \bar{D}^{*0}\tau^+\nu_\tau$  was observed with a significance of  $8.1\sigma$ , and evidence for  $B^+ \rightarrow \bar{D}^0\tau^+\nu_\tau$  was established at  $3.5\sigma$ . The event distributions and fits are shown in Fig. 2(b-e).

#### 4.1.2. Belle hadronic-tagging Measurement

Belle performed a hadronic-tagging analysis of the four channels  $B^0 \rightarrow D^-\tau^+\nu_\tau$ ,  $B^0 \rightarrow D^{*-}\tau^+\nu_\tau$ ,  $B^+ \rightarrow \bar{D}^0\tau^+\nu_\tau$ , and  $B^+ \rightarrow \bar{D}^{*0}\tau^+\nu_\tau$ , using  $657 \times 10^6 B\bar{B}$  pairs. The results were reported at a conference<sup>43</sup> in 2009, but have not been published. Signal- $B$  reconstruction was performed in the two leptonic decays  $\tau^+ \rightarrow \ell^+\nu_\ell\bar{\nu}_\tau$ , a

total of 10  $D$ -meson decay modes, and 4  $D^*$  modes. The tag- $B$  was reconstructed only in the two-body decays  $\bar{B} \rightarrow D^{(*)}h^-$ , where  $h^-$  was a  $\pi^-$ ,  $\rho^-$ ,  $a_1^-$ , or  $D_s^{(*)-}$ , with a total of 15  $D_{(s)}$  decay modes and 5  $D_{(s)}^*$  modes.

The yield of  $B \rightarrow \bar{D}^{(*)}\ell^+\nu_\ell$  events in each of the four modes was obtained by fitting the  $m_{\text{miss}}^2$  distribution in the control sample defined by  $|m_{\text{miss}}^2| < 1 \text{ GeV}^2$ . The signal yields were obtained from a two-dimensional fit to the distribution of  $m_{\text{miss}}^2$  vs.  $E_{\text{extra}}$  in the range  $-2 < m_{\text{miss}}^2 < 8 \text{ GeV}^2$ . The two fit variables were found to be uncorrelated for  $B \rightarrow \bar{D}^{(*)}\tau^+\nu_\tau$  and  $B \rightarrow \bar{D}^{(*)}\ell^+\nu_\ell$ , and the correlation for the remaining background types was accounted for using simulated events. The distributions of these variables and the fit functions are shown in Fig. 3. The ratio  $R(D^{(*)})$  was extracted from the two yields, accounting for the different  $B \rightarrow \bar{D}^{(*)}\ell^+\nu_\ell$  efficiencies in the two samples. The results of the fits are summarized in Table 1.

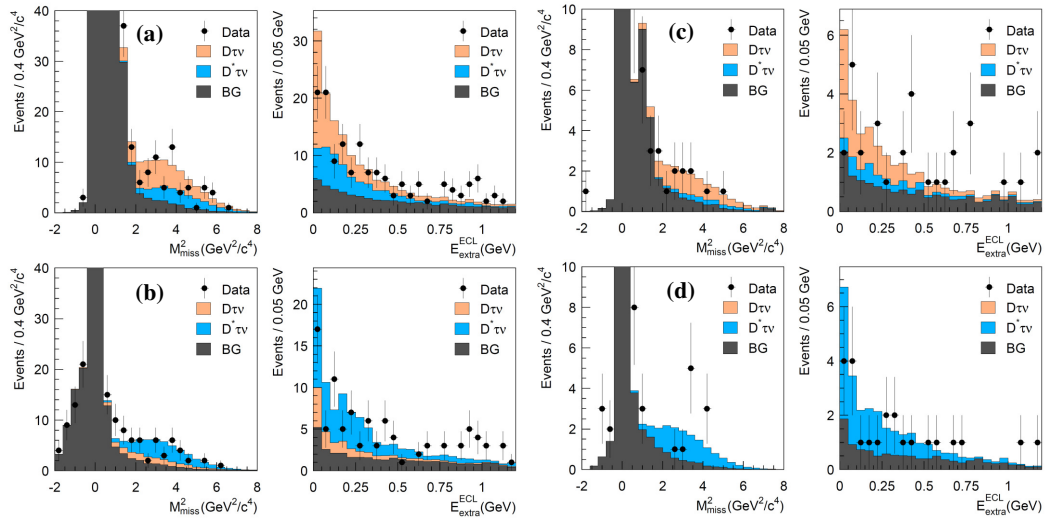


Fig. 3. Distributions of  $m_{\text{miss}}^2$  and  $E_{\text{extra}}$  (the left and right figures, respectively, in each labeled pair of plots) for  $B^+ \rightarrow \bar{D}^{*0}\tau^+\nu_\tau$  (a),  $B^+ \rightarrow \bar{D}^{*0}\tau^+\nu_\tau$  (b),  $B^0 \rightarrow D^-\tau^+\nu_\tau$  (c), and  $B^0 \rightarrow D^{*-}\tau^+\nu_\tau$  (d) candidates in the preliminary Belle analysis<sup>43</sup>. Shaded histograms show the fit results.

#### 4.1.3. BABAR Hadronic-Tagging Measurement

In 2008, *BABAR* reported the first study of the four  $B \rightarrow \bar{D}^{(*)}\tau^+\nu_\tau$  channels using a sample of  $232 \times 10^6$   $B\bar{B}$  pairs. The decay  $B^+ \rightarrow \bar{D}^{*0}\tau^+\nu_\tau$  was observed with a significance of  $5.3\sigma$ , and evidence for  $B^0 \rightarrow D^-\tau^+\nu_\tau$  was obtained at  $3.3\sigma$ . Rather than describing this analysis in detail, we do so for the 2012 analysis<sup>13,14</sup> that superseded it, and which used a larger data sample ( $471 \times 10^6$   $B\bar{B}$  pairs) and improved hadronic tagging. (see discussion in Sec. 3.1).

Table 1. Results of the preliminary  $B \rightarrow \bar{D}^{(*)}\tau^+\nu_\tau$  analysis from Belle<sup>43</sup>, showing for each mode the number of signal events, the ratio  $R(D^{(*)})$ , the branching fraction, and the signal significance. Where given, the third uncertainty is due to the branching fraction  $\mathcal{B}(B \rightarrow \bar{D}^{(*)}\ell^+\nu_\ell)$ .

Decay mode	$N_{\text{signal}}$	$R(D^{(*)})$	$\mathcal{B}(\%)$	Significance
$B^+ \rightarrow \bar{D}^0\tau^+\nu_\tau$	$98.6^{+26.3}_{-25.0}$	$0.70^{+0.19+0.11}_{-0.18-0.09}$	$1.51^{+0.41+0.24}_{-0.39-0.19} \pm 0.15$	3.8
$B^0 \rightarrow D^-\tau^+\nu_\tau$	$17.2^{+7.7}_{-6.9}$	$0.48^{+0.22+0.06}_{-0.19-0.05}$	$1.01^{+0.46+0.13}_{-0.41-0.11} \pm 0.10$	2.6
$B^+ \rightarrow \bar{D}^{*0}\tau^+\nu_\tau$	$99.8^{+22.2}_{-21.3}$	$0.47^{+0.11+0.06}_{-0.10-0.07}$	$3.04^{+0.69+0.40}_{-0.66-0.47} \pm 0.22$	3.9
$B^0 \rightarrow D^{*-}\tau^+\nu_\tau$	$25.0^{+7.2}_{-6.3}$	$0.48^{+0.14+0.06}_{-0.12-0.04}$	$2.56^{+0.75+0.31}_{-0.66-0.22} \pm 0.10$	4.7

Tag- $B$  reconstruction in the 2012 analysis was performed with 1680 final states. Signal- $B$  decays were reconstructed in the two  $\tau^+$  leptonic modes, 11  $D$  modes, and four  $D^*$  modes. The final analysis stage was a simultaneous fit to the two-dimensional distributions of  $m_{\text{miss}}^2$  vs. the lepton momentum  $p_\ell^*$  in the signal- $B$  rest frame. The correlation between these variables necessitated evaluation of the two-dimensional fit functions from simulated events. The fit was performed simultaneously on the four  $B \rightarrow \bar{D}^{(*)}\tau^+\nu_\tau$  candidate samples plus four control samples, in which an additional  $\pi^0$  was reconstructed in an attempt to identify production of a  $D^{**}$ , defined here as an excited charm state heavier than the  $D^*$ . The control samples helped determine the contribution of poorly understood  $B \rightarrow \bar{D}^{**}\ell^+\nu_\ell$  and  $B \rightarrow \bar{D}^{**}\tau^+\nu_\tau$  backgrounds to the  $B \rightarrow \bar{D}^{(*)}\tau^+\nu_\tau$  candidate samples. The ratios of the  $B \rightarrow \bar{D}^{(*)}\tau^+\nu_\tau$  and  $B \rightarrow \bar{D}^{(*)}\ell^+\nu_\ell$  yields were used to calculate  $R(D^{(*)})$ , and earlier BABAR measurements<sup>44,45,46</sup> of  $\mathcal{B}(B \rightarrow \bar{D}^{(*)}\ell^+\nu_\ell)$  were used to obtain  $\mathcal{B}(B \rightarrow \bar{D}^{(*)}\tau^+\nu_\tau)$ .

The analysis resulted in the first significant observation of  $B \rightarrow \bar{D}\tau^+\nu_\tau$ . The  $m_{\text{miss}}^2$  and  $p_\ell^*$  distributions of the data are shown in Fig. 4, overlaid with the fit function when the isospin constraint  $R(D^{(*)0}) = R(D^{(*)+}) \equiv R(D^{(*)})$  was applied. The results are presented in Table 2 for each of the four decay modes and for the isospin-constrained fit.

BABAR found the measured values of  $R(D)$  and  $R(D^*)$  to be higher by  $2.0\sigma$  and  $2.7\sigma$ , respectively, than the SM expectation (Eq. (5)). Accounting for correlations between the  $R(D)$  and  $R(D^*)$  measurements, the combined consistency with the SM was  $3.4\sigma$ , corresponding to a  $p$ -value of  $6.9 \times 10^{-4}$ . This is reduced to  $3.2\sigma$  when using Eq. (6), with similar results obtained for Eq. (7). The measured branching fractions for the four modes are higher than the predictions of Eq. (8), by 1.4, 1.7, 1.3, and 1.9 standard deviations, respectively. The  $q^2$  spectra were found to be consistent with the SM to within the statistical uncertainties.

#### 4.1.4. Summary and Consistency of $B \rightarrow \bar{D}^{(*)}\tau^+\nu_\tau$ Measurements

As shown discussed above, the  $B \rightarrow \bar{D}^{(*)}\tau^+\nu_\tau$  rate measurements have consistently yielded results higher than the SM expectations. Comparison of theory and experimental results from both BABAR and Belle is best performed in terms of the

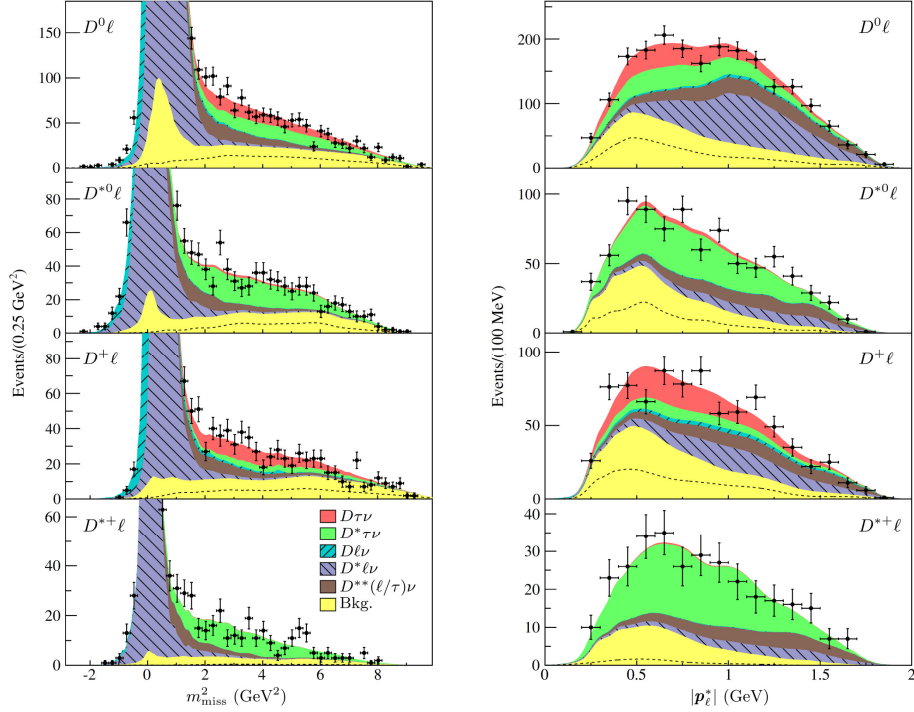


Fig. 4.  $m_{\text{miss}}^2$  (left) and  $p_l^*$  (right) distributions of the  $B \rightarrow \bar{D}^{(*)}\tau^+\nu_\tau$  candidates reconstructed by BABAR<sup>13,14</sup>. Shaded regions show the results of the fit with the isospin constraint  $R(D^{(*)0}) = R(D^{(*)+}) \equiv R(D^{(*)})$ . The reconstructed final state is shown on each plot. The  $p_l^*$  distributions were produced with the requirement  $m_{\text{miss}}^2 > 1 \text{ GeV}^2$  to suppress the large  $B \rightarrow \bar{D}^{(*)}\ell^+\nu_\ell$  peak, which is truncated in the  $m_{\text{miss}}^2$  distributions. The dashed line shows the level of the continuum background.

Table 2. Results of the  $B \rightarrow \bar{D}^{(*)}\tau^+\nu_\tau$  analysis from BABAR<sup>13,14</sup>, showing for each mode the number of signal events, the ratio  $R(D^{(*)})$ , the branching fraction, and the signal significance.

Decay mode	$N_{\text{signal}}$	$R(D^{(*)})$	$\mathcal{B}(\%)$	Significance ( $\sigma$ )
$B^+ \rightarrow \bar{D}^0\tau^+\nu_\tau$	$314 \pm 60$	$0.429 \pm 0.082 \pm 0052$	$0.99 \pm 0.19 \pm 0.13$	4.7
$B^0 \rightarrow D^-\tau^+\nu_\tau$	$177 \pm 31$	$0.469 \pm 0.084 \pm 0053$	$1.01 \pm 0.18 \pm 0.12$	5.2
$B^+ \rightarrow \bar{D}^{*0}\tau^+\nu_\tau$	$639 \pm 62$	$0.322 \pm 0.032 \pm 0022$	$1.71 \pm 0.17 \pm 0.13$	9.4
$B^0 \rightarrow D^{*-}\tau^+\nu_\tau$	$245 \pm 27$	$0.355 \pm 0.039 \pm 0021$	$1.74 \pm 0.19 \pm 0.12$	10.4
$B \rightarrow \bar{D}\tau^+\nu_\tau$	$489 \pm 63$	$0.440 \pm 0.058 \pm 0042$	$1.02 \pm 0.13 \pm 0.11$	6.8
$B \rightarrow \bar{D}^*\tau^+\nu_\tau$	$888 \pm 63$	$0.332 \pm 0.024 \pm 0018$	$1.76 \pm 0.13 \pm 0.12$	13.2

branching-fraction ratios  $R(D^{(*)})$ . However, this is complicated by the fact that the published Belle results were given in terms of the branching fractions, and corre-

lations between the  $R(D)$  and  $R(D^*)$  results in the Belle measurements have not been published. An unofficial combination of the published<sup>41,42</sup> and preliminary<sup>43</sup> Belle results with the *BABAR* results<sup>13,14</sup> has been performed<sup>47</sup> in terms of  $R(D^{(*)})$ . This calculation found the combined Belle results for  $R(D^{(*)})$  to be within  $3.3\sigma$  of the SM prediction. Combining results from both experiments yielded a discrepancy of  $4.8\sigma$  with respect to the SM.

Lastly, we check the consistency of the  $B$ -factory results with the ALEPH measurement<sup>48</sup> of the inclusive branching fraction

$$\mathcal{B}(b_Z \rightarrow D^{*-} \tau^+ \nu_\tau X) = (0.88 \pm 0.31 \pm 0.28)\%, \quad (21)$$

where  $X$  stands for possible additional particles, and  $b_Z$  indicates a  $b$  quark produced in  $Z^0 \rightarrow b\bar{b}$ . The fraction of these quarks that hadronize into  $B^+$  or  $B^0$  mesons is  $f_{Z \rightarrow B} = (80.8 \pm 1.8)\%$ , where equal production of both meson types is assumed<sup>49</sup>. The remaining  $\sim 20\%$  hadronize into  $B_s$  mesons and  $b$  baryons, which undergo semileptonic decays that tend to produce  $D_s$  mesons and charmed baryons, respectively<sup>25</sup>, rather than  $D^{*-}$  mesons. Therefore, the dominant source of  $D^{*-} \tau^+ \nu_\tau X$  events in the ALEPH measurement was  $B^+$  and  $B^0$  decays. We note that<sup>25</sup>

$$\mathcal{B}(B^0 \rightarrow D^{*-} \ell^+ \nu_\ell) \approx \mathcal{B}(B^+ \rightarrow D^{(*)}(n\pi) \ell^+ \nu_\ell) + \mathcal{B}(B^0 \rightarrow D^{(*)}(n\pi) \ell^+ \nu_\ell), \quad (22)$$

where  $(n\pi)$  stands for at least one pion. Assuming this approximate relation holds for decays with a  $\tau^+$  lepton in the final state, one obtains the expectation

$$\mathcal{B}(b_Z \rightarrow D^{*-} \tau^+ \nu_\tau X) \approx \frac{f_{Z \rightarrow B}}{2} \left( 1 + F_{D^{*-}} \frac{R(D^{*}(n\pi))}{R(D^*)} \right) \mathcal{B}(B^0 \rightarrow D^{*-} \tau^+ \nu_\tau), \quad (23)$$

where  $F_{D^{*-}}$  is the fraction of decays on the right-hand side of Eq. (22) in which a  $D^{*-}$  is produced, and  $R(D^{*}(n\pi)) \equiv \mathcal{B}(B \rightarrow D^{*}(n\pi) \tau^+ \nu_\tau) / \mathcal{B}(B \rightarrow D^{*}(n\pi) \ell^+ \nu_\ell)$ . Given the fraction of  $D^{*-}$  production in  $B \rightarrow \bar{D}^{(*)} \ell^+ \nu_\ell$  decays<sup>25</sup>, we take  $F_{D^{*-}}$  to be between  $1/4$  and  $1/2$ . Phase-space considerations suggest  $R(D^{*}(n\pi)) < R(D^*)$ , but to be conservative, we take this relation to be an equality. Then with the value of  $\mathcal{B}(B^0 \rightarrow D^{*-} \tau^+ \nu_\tau)$  from Table 2, Eq.(23) predicts  $\mathcal{B}(b_Z \rightarrow D^{*-} \tau^+ \nu_\tau X)$  to be between 0.9 and 1.0, with the range being due to our choices for  $F_{D^{*-}}$ . This is in excellent agreement with the measured value, Eq.(21).

#### 4.2. $B^+ \rightarrow \tau^+ \nu_\tau$ Measurements

Prior to the start of the  $B$  factory programs, searches for  $B^+ \rightarrow \tau^+ \nu_\tau$  were conducted by ARGUS<sup>50</sup>, CLEO<sup>51,52</sup>, ALEPH<sup>53,48</sup>, and L3<sup>54</sup>, reaching a limit of  $\mathcal{B}(B^+ \rightarrow \tau^+ \nu_\tau) < 5.7 \times 10^{-4}$ . Between 2004 and 2013, *BABAR* and Belle published a total of nine papers on the topic, using both semileptonic tagging<sup>55,56,39,57,58</sup> and hadronic tagging<sup>59,60,38,61</sup>. First evidence for this decay, at a level of  $3.5\sigma$ , was obtained by Belle with hadronic tagging<sup>59</sup> and a data sample containing  $449 \times 10^6$   $B\bar{B}$  pairs, and resulted in a branching-fraction measurement of  $\mathcal{B}(B^+ \rightarrow \tau^+ \nu_\tau) =$

$(1.79^{+0.56+0.45}_{-0.49-0.51}) \times 10^{-4}$ . Results became more precise as the data samples grew and analysis methods improved.

In what follows, we describe the four most recent  $B$ -factory measurements of  $\mathcal{B}(B^+ \rightarrow \tau^+ \nu_\tau)$ . A summary of the experimental results and how they compare to the SM expectation is given in Sec. 4.2.3.

#### 4.2.1. Semileptonic-Tagging Measurements

In 2010, *BABAR* and Belle published studies of  $B^+ \rightarrow \tau^+ \nu_\tau$  with semileptonic tagging. The *BABAR* analysis<sup>57</sup> used a data sample of  $459 \times 10^6$   $B\bar{B}$  pairs. They reconstructed the tag  $B$  in the decays  $B^- \rightarrow D^0 \ell^- \bar{\nu}_\ell X$ , where  $X$  stands for possible additional particles that were not reconstructed. The  $\tau^+$  was reconstructed in the leptonic decays  $\tau^+ \rightarrow \ell^+ \nu_\ell \bar{\nu}_\tau$  and the hadronic decays  $\tau^+ \rightarrow \pi^+ \bar{\nu}_\tau$  and  $\tau^+ \rightarrow \rho^+ \bar{\nu}_\tau$ . The signal yield in each  $\tau^+$  channel was measured from the number of events in the signal region  $E_{\text{extra}} < 0.4$  GeV, after subtraction of the expected background yield. This, in turn, was obtained from the simulated  $E_{\text{extra}}$  distribution, normalized to the sideband  $E_{\text{extra}} > 0.4$  GeV. The simulation predictions for the  $E_{\text{extra}}$  distributions of the background were validated using a double-tag control sample, in which both  $B$  mesons were reconstructed via semileptonic decays. *BABAR* observed 583 signal-region events with a background expectation of  $509 \pm 30$  events, and reported the branching fraction  $\mathcal{B}(B^+ \rightarrow \tau^+ \nu_\tau) = (1.7 \pm 0.8 \pm 0.2) \times 10^{-4}$ , with a signal significance of  $2.3\sigma$ . A mode-by-mode breakdown of the results is shown in Table 3, and the  $E_{\text{extra}}$  distributions are shown in Figs. 5(a-e).

Table 3. Results of the semileptonic-tagging  $B^+ \rightarrow \tau^+ \nu_\tau$  analyses from *BABAR*<sup>57</sup> and Belle<sup>58</sup>, showing the expected number of background events ( $N_{\text{background}}$ ) and the number of observed events ( $N_{\text{observed}}$ ) in the signal region for *BABAR*, the number of signal events ( $N_{\text{signal}}$ ) obtained from the fit for Belle, and the branching fraction  $\mathcal{B}(B^+ \rightarrow \tau^+ \nu_\tau)$  for both experiments.

Decay mode	<i>BABAR</i> results			Belle results	
	$N_{\text{background}}$	$N_{\text{observed}}$	$\mathcal{B}(\times 10^{-4})$	$N_{\text{signal}}$	$\mathcal{B}(\times 10^{-4})$
$\tau^+ \rightarrow e^+ \nu_e \bar{\nu}_\tau$	$81 \pm 12$	121	$3.6 \pm 1.4$	$73^{+23}_{-22}$	$1.90^{+0.59+0.33}_{-0.57-0.35}$
$\tau^+ \rightarrow \mu^+ \nu_\mu \bar{\nu}_\tau$	$135 \pm 13$	148	$1.3^{+1.8}_{-1.6}$	$12^{+18}_{-17}$	$0.5^{+0.76+0.18}_{-0.72-0.21}$
$\tau^+ \rightarrow \pi^+ \nu_e \bar{\nu}_\tau$	$234 \pm 19$	243	$0.6^{+1.4}_{-1.2}$	$55^{+21}_{-20}$	$1.80^{+0.69+0.36}_{-0.66-0.37}$
$\tau^+ \rightarrow \rho^+ \nu_e \bar{\nu}_\tau$	$59 \pm 9$	71	$2.1^{+2.0}_{-1.8}$		
Combined	$509 \pm 30$	583	$1.7 \pm 0.8 \pm 0.2$	$143^{+36}_{-35}$	$1.54^{+0.38+0.29}_{-0.37-0.31}$

The Belle semileptonic-tagging analysis used a data sample of  $657 \times 10^6$   $B\bar{B}$  pairs. The  $\tau^+$  was reconstructed in  $\tau^+ \rightarrow \ell^+ \nu_\ell \bar{\nu}_\tau$  and  $\tau^+ \rightarrow \pi^+ \bar{\nu}_\tau$ . A fit to the

<sup>c</sup>Figs. 2(f-i) are reprinted with permission from K. Hara *et al.*, Phys. Rev. D **82**, 071101 (2010). Copyright (2010) by the American Physical Society.

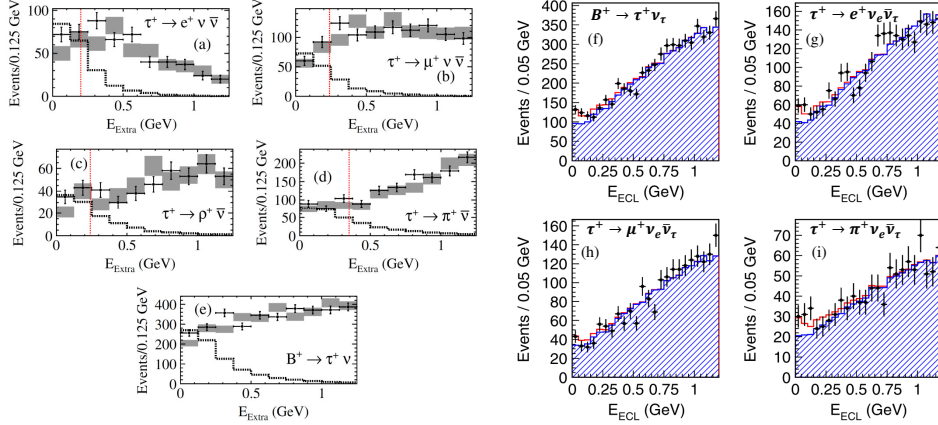


Fig. 5.  $E_{\text{extra}}$  distributions in the *BABAR* semileptonic-tagging  $B^+ \rightarrow \tau^+ \nu_\tau$  analysis<sup>57</sup>, shown for each  $\tau^+$  decay mode (a-d) and for the sum of the modes (e). The grey boxes show the background expectation from simulation, normalized to the sideband  $E_{\text{extra}} < 0.4$  GeV indicated by the dotted vertical line. The dotted histogram is ten times the expected signal contribution. Also shown are  $E_{\text{extra}}$  distributions in the corresponding Belle analysis<sup>58</sup> for each mode (g-i) and for the sum of the modes (f). The hatched blue histogram is the background expectation,<sup>2</sup> and the solid red histogram includes the signal contribution.

$E_{\text{extra}}$  distribution provided the yields of signal and background events for each  $\tau^+$  decay mode. The fit functions were obtained from simulation, corrected using control samples of double-tag events and data taken off the  $\Upsilon(4S)$  resonance. The  $E_{\text{extra}}$  distributions and fit functions are shown in Fig. 5(f-i), and the signal yield and branching fraction obtained for each mode are listed in Table 3. Combining the four  $\tau^+$  mode, Belle found  $143_{-35}^{+36}$  signal events, a signal significance of  $3.6\sigma$ , and a branching-fraction measurement of  $\mathcal{B}(B^+ \rightarrow \tau^+ \nu_\tau) = (1.54_{-0.37}^{+0.48} {}_{-0.31}^{+0.29}) \times 10^{-4}$ .

#### 4.2.2. Hadronic-Tagging Measurements

In 2013, *BABAR* and Belle published  $B^+ \rightarrow \tau^+ \nu_\tau$  results based on their full data sets and improved hadronic tagging methods (see Sec. 3.1), leading to significant improvements over previous hadronic-tagging results. Both analyses used the four decay modes  $\tau^+ \rightarrow \ell^+ \nu_\ell \bar{\nu}_\tau$ ,  $\pi^+ \bar{\nu}_\tau$ , and  $\rho^+ \bar{\nu}_\tau$ .

The *BABAR* analysis<sup>61</sup> was performed with a data sample of  $467.8 \times 10^6 B\bar{B}$  pairs. A simultaneous fit to the  $E_{\text{extra}}$  distributions of all modes was used to extract the signal branching fraction and the background yield in each mode. The fit functions for events with a correctly reconstructed  $B_{\text{tag}}$  were taken from simulation after corrections for data-simulation discrepancies obtained from double-tag events, in which the signal  $B$  was replaced by a  $B$  meson reconstructed via a hadronic or semileptonic decay. The fit functions for the combinatorial background were histograms of data events in the sideband  $5.209 < m_{\text{ES}} < 5.260$  GeV. The  $E_{\text{extra}}$  distributions are shown in Fig. 6, and the results are summarized in Table 4. *BABAR* found a total



of  $62.1 \pm 17.3$  signal events and a significance of  $3.8\sigma$ , and measured the branching fraction  $\mathcal{B}(B^+ \rightarrow \tau^+ \nu_\tau) = (1.83_{-0.49}^{+0.53} \pm 0.24) \times 10^{-4}$ .

Table 4. Results of the hadronic-tagging  $B^+ \rightarrow \tau^+ \nu_\tau$  analyses from BABAR<sup>61</sup> and Belle<sup>38</sup>, showing the signal yield and the calculated branching fraction for each  $\tau^+$  mode and for the combination of the modes.

Decay mode	BABAR results		Belle results	
	$N_{\text{signal}}$	$\mathcal{B}(\times 10^{-4})$	$N_{\text{signal}}$	$\mathcal{B}(\times 10^{-4})$
$\tau^+ \rightarrow e^+ \nu_e \bar{\nu}_\tau$	$4.1 \pm 9.1$	$0.35_{-0.73}^{+0.84}$	$16_{-9}^{+11}$	$0.68_{-0.41}^{+0.49}$
$\tau^+ \rightarrow \mu^+ \nu_\mu \bar{\nu}_\tau$	$12.9 \pm 9.7$	$1.12_{-0.78}^{+0.90}$	$26_{-14}^{+15}$	$1.06_{-0.58}^{+0.63}$
$\tau^+ \rightarrow \pi^+ \nu_e \bar{\nu}_\tau$	$17.1 \pm 6.2$	$3.69_{-1.22}^{+1.42}$	$8_{-8}^{+10}$	$0.57_{-0.59}^{+0.70}$
$\tau^+ \rightarrow \rho^+ \nu_e \bar{\nu}_\tau$	$24.0 \pm 10.0$	$3.78_{-1.45}^{+1.65}$	$14_{-16}^{+19}$	$0.52_{-0.62}^{+0.72}$
Combined	$62.1 \pm 17.3$	$1.83_{-0.49}^{+0.53} \pm 0.24$	$62_{-22}^{+23}$	$0.72_{-0.25}^{+0.27} \pm 0.11$

The Belle hadronic-tagging analysis<sup>38</sup> made use of  $772 \times 10^6$   $B\bar{B}$  pairs. The signal yield was obtained from a two-dimensional fit to the distribution of  $E_{\text{extra}}$  vs.  $m_{\text{miss}}^2$ . The distributions of the two variables were found to be uncorrelated, except for  $\tau^+ \rightarrow \rho^+ \bar{\nu}_\tau$  events reconstructed as  $\tau^+ \rightarrow \pi^+ \bar{\nu}_\tau$ , for which the correlation was taken into account in the fit function. Double-tagged events were used to validate the signal fit functions. The  $E_{\text{extra}}$  and  $m_{\text{miss}}^2$  distributions of the data and the corresponding fit functions are shown in Fig. 6, and the fit results are shown in Table 4. The total signal yield was  $62_{-22}^{+23}$  events, and the branching fraction was found to be  $\mathcal{B}(B^+ \rightarrow \tau^+ \nu_\tau) = 0.72_{-0.25}^{+0.27} \pm 0.11$ , with a signal significance of  $3.0\sigma$ .

#### 4.2.3. Summary of $B^+ \rightarrow \tau^+ \nu_\tau$ Results

As the  $B$ -factory data samples grew and  $\mathcal{B}(B^+ \rightarrow \tau^+ \nu_\tau)$  results became more precise, tension was building between the experimental average and the SM expectations based on  $|V_{ub}|$  from exclusive semileptonic decays or on the unitarity-triangle fits. For example, the CKMfitter<sup>27</sup> expectation for  $\mathcal{B}(B^+ \rightarrow \tau^+ \nu_\tau)$ , Eq. (14), differed by  $2.6\sigma$  from the experimental world average of  $(1.65 \pm 0.34) \times 10^{-4}$  before the 2013 hadronic-tagging measurement from Belle<sup>38</sup>. This new measurement now dominates the world average of  $(1.15 \pm 0.23) \times 10^{-4}$ , which is only  $1.7\sigma$  from the CKMfitter expected value. While the new world average is  $2.4\sigma$  from the predicted value of  $R'$  (Eq. (15)), at the more relevant high values of  $q^2$ , the difference is reduced<sup>33</sup> to  $1.6\sigma$ .

Fig. 7 summarizes the results and their averages before and after the 2013 Belle measurement, comparing them with two SM expectation values: one based on  $V_{ub}$  from the direct measurement, and the other from CKMfitter. Finally, we note that the naïve significance of the world average for  $\mathcal{B}(B^+ \rightarrow \tau^+ \nu_\tau)$  is  $1.15/0.23 = 5\sigma$ .

<sup>b</sup>Figs. 2(f-g) are reprinted with permission from I. Adachi *et al.*, Phys. Rev. Lett. **110**, 131801 (2013). Copyright (2013) by the American Physical Society.

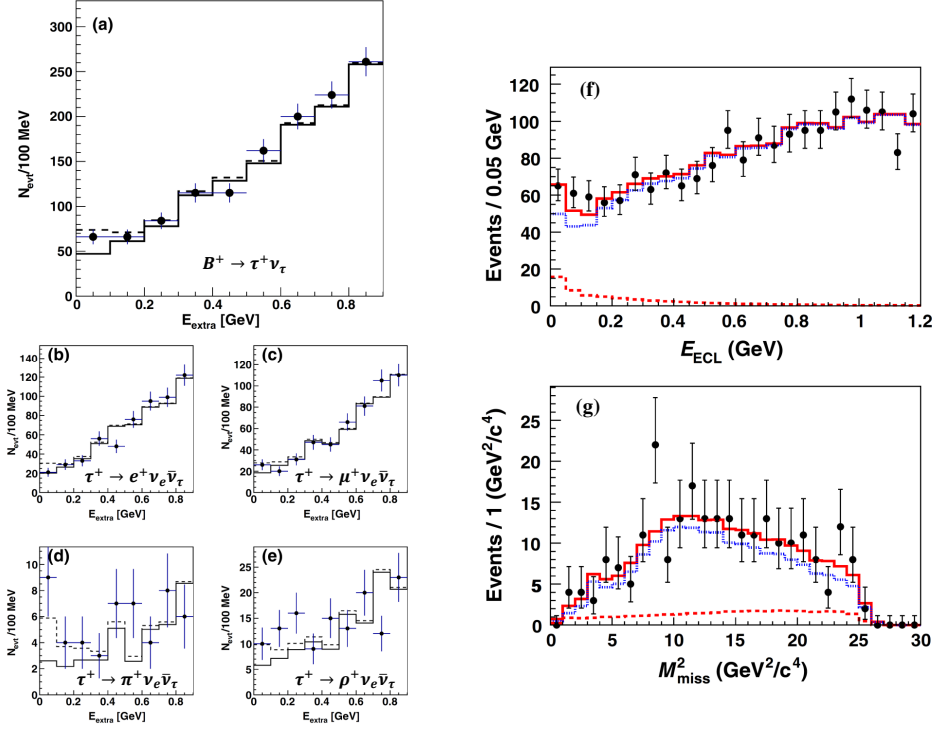


Fig. 6.  $E_{\text{extra}}$  distributions in the *BABAR* hadronic-tagging  $B^+ \rightarrow \tau^+ \nu_\tau$  analysis<sup>61</sup>, shown for the sum of the  $\tau^+$  modes (a) and for each mode separately (b-e). The solid histograms show the background contributions, and the dashed histograms show the background-plus-signal fit functions. The  $E_{\text{extra}}$  (f) and  $m_{\text{miss}}^2$  (g) distributions in the corresponding Belle analysis<sup>38</sup> are shown for the sum of the modes. The dotted blue histograms are the background contribution, the red dashed histograms show the signal contribution, and the solid red is the total fit function.

## 5. New-Physics Interpretation of the Results

Given that  $\mathcal{B}(B^+ \rightarrow \tau^+ \nu_\tau)$  has now come into agreement with the SM expectation, we focus the discussion on possible NP contributions to  $B \rightarrow \bar{D}^{(*)} \tau^+ \nu_\tau$ , where the discrepancy between theory and experiment has recently increased.

The most thorough interpretation of a  $B \rightarrow \bar{D}^{(*)} \tau^+ \nu_\tau$  measurement in terms of NP constraints was conducted by *BABAR* for their results<sup>13,14</sup>. Within a type-II 2HDM (Eq. (10)), they extracted  $\tan \beta / m_{H^+} = 0.44 \pm 0.02 \text{ GeV}^{-1}$  from  $R(D)$  and  $\tan \beta / m_{H^+} = 0.75 \pm 0.04 \text{ GeV}^{-1}$  from  $R(D^*)$ . From the disagreement between these results, they ruled out the model with a confidence level of at least 99.8% for any value of  $\tan \beta / m_{H^+}$  (this includes the SM point of  $\tan \beta / m_{H^+} = 0$ , see Sec. 4.1.3), excluding a much broader range of parameters than recent (albeit low-luminosity) LHC searches for a charged Higgs boson<sup>62,63</sup>. A similar analysis has not been performed for the Belle  $B \rightarrow \bar{D}^{(*)} \tau^+ \nu_\tau$  measurements. However, given the agreement of the results of the two experiments, one can expect that combining

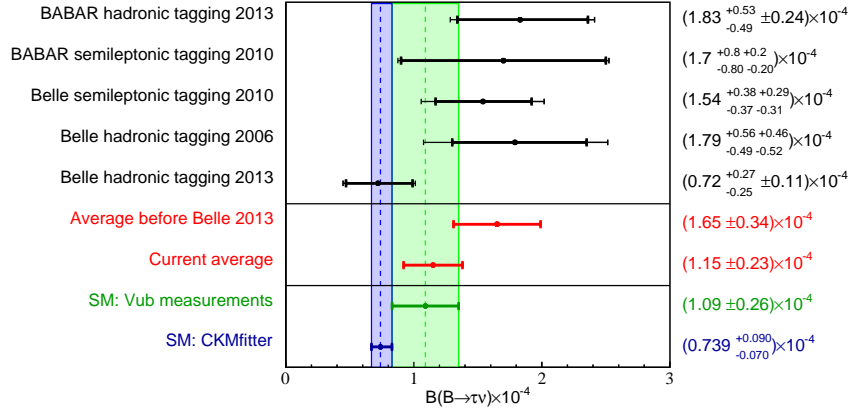


Fig. 7. Summary of the latest  $\mathcal{B}(B^+ \rightarrow \tau^+ \nu_\tau)$  measurements, with the experiment, tagging method, and publication year indicated. Inner (outer) error bars show the statistical (total) uncertainties. Also shown are the PDG world average<sup>25</sup> before the 2013 Belle measurement<sup>38</sup> and the current PDG average, which was substantially lowered by that measurement. Two SM expectations are shown as vertical bands: using either the PDG average of  $|V_{ub}|$  measurements (Eq. (13)) or the CKMfitter value (Eq. (14)).

their results would yield even tighter limits on the parameter space.

*BABAR* also analyzed their  $R(D^{(*)})$  results in the context of a type-III 2HDM, restricting the analysis to real values of the parameters  $S_R$  and  $S_L$  of Eq. (9). They found four favored regions in the two-dimensional plane, shown in Fig. 8. Additional constraints were obtained by considering the  $q^2$  distributions, in particular for  $B \rightarrow \bar{D}\tau^+\nu_\tau$ , which tends to shift to higher values in the presence of a scalar contribution. For the two favored regions shown in Fig. 8 at  $\Re(S_R + S_L) \sim -1.5$ , the expected  $q^2$  distribution is significantly harder than the spectrum measured in the data. As a result, these regions were excluded with a significance of at least  $2.9\sigma$ . Thus, only the two regions at  $\Re(S_R + S_L) \sim 0.4$  were favored by the measurement. However, *BABAR* noted that the  $q^2$  spectra of the data were in better agreement with the SM than with these regions, or with with 2HDM solutions with complex values of  $S_R$  and  $S_L$ .

A number of authors have analyzed the  $R(D^{(*)})$  results in terms of NP contributions. As an example, we quote some of the results of Tanaka and Watanabe<sup>7</sup>, which were based on their combination of the *BABAR* and Belle results,  $R(D) = 0.305 \pm 0.012$ ,  $R(D^*) = 0.252 \pm 0.004$ . In this model-independent analysis, they used the full effective Hamiltonian of Eq. (1). The constraints they extracted on the coefficients  $V_{L,R}$ ,  $S_{L,R}$ , and  $T_L$  are shown in Fig. 9, under the assumption that only one of the coefficients is non-zero. Model-independent constraints allowing more than one coefficient to vary at a time<sup>64</sup> or focusing on the tensor operator<sup>65</sup> have also been calculated. Additional constraints have been determined for specific models, including leptoquark scenarios<sup>33,66,67</sup>, chiral  $U(1)'$  models<sup>68</sup>, R-parity violation<sup>69</sup>,

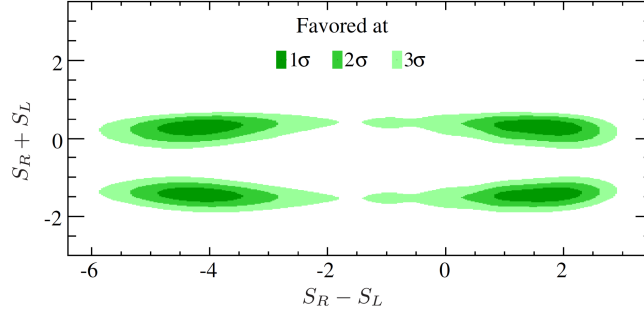


Fig. 8. Favored regions for real values of the type-III 2HDM parameters  $S_R$  and  $S_L$  given the *BABAR* results<sup>13,14</sup> for  $R(D^{(*)})$ . Further analysis of the  $q^2$  distributions disfavors the two regions at  $\Re(S_R + S_L) \sim -1.5$  with a significance of at least  $2.9\sigma$ .

sterile neutrinos<sup>70</sup>, and nonuniversal left-right models<sup>71</sup>.

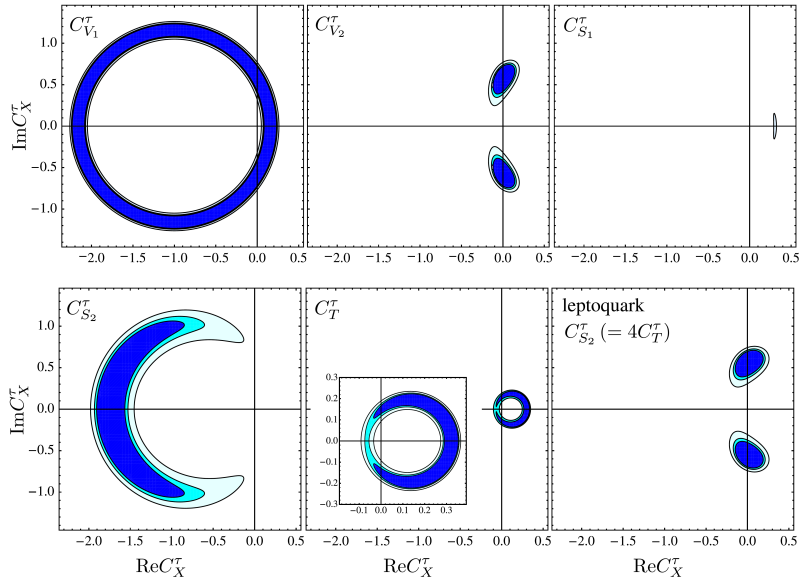


Fig. 9. 90% (light blue), 95% (cyan), and 99% (dark blue) confidence-level favored regions for the coefficients of Eq. (1), assuming that only one coefficient is non-zero<sup>7</sup>. The conversion to the notation of Eq. (1) is  $C_{V_1}^\tau = V_L$ ,  $C_{V_2}^\tau = V_R$ ,  $C_{S_1}^\tau = S_R$ ,  $C_{S_2}^\tau = S_L$ ,  $C_T^\tau = T_L$ . The bottom-right panel corresponds to a scalar leptoquark scenario, where  $C_{S_2}^\tau = 4C_T^\tau$ .

<sup>a</sup>Fig. 9 is reprinted with permission from M. Tanaka and R. Watanabe, Phys. Rev. D. **87**, 0340281 (2013). Copyright (2013) by the American Physical Society.

## 6. Conclusions and Outlook

Measurements of the branching fractions of the decays  $B^+ \rightarrow \tau^+ \nu_\tau$  and  $B \rightarrow \bar{D}^{(*)} \tau^+ \nu_\tau$  have long been in some tension with the SM expectations. Recent measurements by *BABAR* and Belle have essentially removed the tension<sup>38</sup> in  $B^+ \rightarrow \tau^+ \nu_\tau$  and increased it in  $B \rightarrow \bar{D}^{(*)} \tau^+ \nu_\tau$  to a level of at least  $3.2\sigma$ <sup>13,14</sup> and perhaps as much as  $4.8\sigma$ <sup>47</sup>. The  $B \rightarrow \bar{D}^{(*)} \tau^+ \nu_\tau$  results disfavor<sup>13</sup> type-II two-Higgs-doublet models with a confidence level of at least 99.8%. Constraints have been calculated on the parameter spaces of other models and on Wilson coefficients within model-independent analyses.

*BABAR* and Belle have used their full data sets and best  $B$ -tagging methods for the  $B^+ \rightarrow \tau^+ \nu_\tau$  measurements. Although further improvements in hadronic  $B$  tagging (Sec. 3.1) would yield some improvement in efficiency, the overall sensitivity will not increase substantially. Therefore, the current agreement of the world average for  $\mathcal{B}(B^+ \rightarrow \tau^+ \nu_\tau)$  with the SM prediction is expected to persist until the next generation of  $B$ -factory experiments.

The situation is different for  $B \rightarrow \bar{D}^{(*)} \tau^+ \nu_\tau$ . Belle has yet to perform the measurement of  $R(D^{(*)})$  with their improved  $B$ -tagging method. It remains to be seen whether this will bring the world average into agreement with the SM or increase the overall discrepancy to beyond 5 standard deviations. *BABAR* and Belle can also reconstruct  $B \rightarrow \bar{D}^{(*)} \tau^+ \nu_\tau$  with semileptonic tagging, as well as obtain further insight into possible new-physics contributions to this decay from an angular analysis or from simpler measurements of forward-backward asymmetries<sup>72</sup>. The LHCb experiment may be able to contribute to the  $R(D^{(*)})$  measurements<sup>12</sup> with the  $\tau$  lepton identified in the decay  $\tau^+ \rightarrow \pi^+ \pi^- \pi^+ \bar{\nu}_\tau$ , if the large hadronic background can be suppressed down to a manageable level.

Dramatic improvement in our understanding of  $B^+ \rightarrow \tau^+ \nu_\tau$  and  $B \rightarrow \bar{D}^{(*)} \tau^+ \nu_\tau$  and of possible new-physics contributions will come from the Belle-II experiment, which will have a data sample of about  $50 \times 10^9$   $B\bar{B}$  pairs in the early-to-mid 2020's. The expected uncertainty on  $\mathcal{B}(B^+ \rightarrow \tau^+ \nu_\tau)$  has been estimated<sup>73</sup> to be  $4 \times 10^{-6}$ , a roughly 6-fold improvement over the current world average. A similar improvement can be expected for  $B \rightarrow \bar{D}^{(*)} \tau^+ \nu_\tau$ . The precise measurements of  $R(D^{(*)})$  will settle the question of whether the current tension with the SM is the result of a fluctuation or new physics. In the latter case, measurements of the  $q^2$  and angular distributions are likely to have the precision needed for differentiating between different new-physics models. Belle-II could also measure  $\mathcal{B}(B \rightarrow \bar{D}^{**} \tau^+ \nu_\tau)$  for specific  $\bar{D}^{**}$  states, and have a dedicated run at the  $e^+e^- \rightarrow B_s \bar{B}_s$  threshold to measure  $\mathcal{B}(B_s \rightarrow D_s^{(*)-} \tau^+ \nu_\tau)$ . These measurements would be by far less precise than those of  $\mathcal{B}(B \rightarrow \bar{D}^{(*)} \tau^+ \nu_\tau)$ , but may turn out to shed light on the roles of both new physics and hadronic processes in  $\bar{b} \rightarrow \bar{c} \tau^+ \nu_\tau$  decays.

## Acknowledgments

I thank David Jaffe and Damir Becirevic for comments on the manuscript, Dana Lindemann for technical assistance, and Andrzej Bozek for clarifications.

## References

1. *BABAR* Collab. (B. Aubert *et al.*), Nucl. Instrum. Meth. A **729**, 615 (2013) [arXiv:1305.3560 [physics.ins-det]].
2. *BABAR* Collab. (B. Aubert *et al.*), Nucl. Instrum. Meth. A **479** (2002) 1 [hep-ex/0105044].
3. Belle Collab. (A. Abashian *et al.*), Nucl. Instrum. Meth. A **479**, 117 (2002).
4. Belle-II Collab. (T. Abe *et al.*), “Belle II Technical Design Report,” arXiv:1011.0352 [physics.ins-det] (2010).
5. S. Faller, T. Mannel and S. Turczyk, Phys. Rev. D **84**, 014022 (2011) [arXiv:1105.3679 [hep-ph]].
6. A. Datta, M. Duraisamy and D. Ghosh, Phys. Rev. D **86**, 034027 (2012) [arXiv:1206.3760 [hep-ph]].
7. M. Tanaka and R. Watanabe, Phys. Rev. D **87**, no. 3, 034028 (2013) [arXiv:1212.1878 [hep-ph]].
8. N. Cabibbo, Phys. Rev. Lett. **10**, 531 (1963).
9. M. Kobayashi and T. Maskawa, Prog. Theor. Phys. **49**, 652 (1973).
10. S. Fajfer, J. F. Kamenik and I. Nisandzic, Phys. Rev. D **85**, 094025 (2012) [arXiv:1203.2654 [hep-ph]].
11. M. Tanaka, Z. Phys. C **67**, 321 (1995) [hep-ph/9411405].
12. J. F. Kamenik and F. Mescia, Phys. Rev. D **78**, 014003 (2008) [arXiv:0802.3790 [hep-ph]].
13. *BABAR* Collab. (J. P. Lees *et al.*), Phys. Rev. Lett. **109**, 101802 (2012) [arXiv:1205.5442 [hep-ex]].
14. J. P. Lees *et al.* [BaBar Collaboration], Phys. Rev. D **88**, 072012 (2013) [arXiv:1303.0571 [hep-ex]].
15. Heavy Flavor Averaging Group Collab. (Y. Amhis *et al.*), arXiv:1207.1158 [hep-ex].
16. M. Tanaka and R. Watanabe, Phys. Rev. D **82**, 034027 (2010) [arXiv:1005.4306 [hep-ph]].
17. J. A. Bailey, A. Bazavov, C. Bernard, C. M. Bouchard, C. DeTar, D. Du, A. X. El-Khadra and J. Foley *et al.*, Phys. Rev. Lett. **109**, 071802 (2012) [arXiv:1206.4992 [hep-ph]].
18. D. Becirevic, N. Kosnik and A. Tayduganov, Phys. Lett. B **716**, 208 (2012) [arXiv:1206.4977 [hep-ph]].
19. Heavy Flavor Averaging Group (D. Asner *et al.*), End Of Year 2009/Winter 2010 averages, <http://www.slac.stanford.edu/xorg/hfag>.
20. K. Nakamura *et al.* [Particle Data Group Collaboration], J. Phys. G **37**, 075021 (2010).
21. Bell Collab. (W. Dungen *et al.*), Phys. Rev. D **82**, 112007 (2010) [arXiv:1010.5620 [hep-ex]].
22. M. Duraisamy and A. Datta, JHEP **1309**, 059 (2013) [arXiv:1302.7031 [hep-ph]].
23. A. Crivellin, C. Greub and A. Kokulu, Phys. Rev. D **86**, 054014 (2012) [arXiv:1206.2634 [hep-ph]].
24. H. Na, C. J. Monahan, C. T. H. Davies, R. Horgan, G. P. Lepage and J. Shigemitsu, Phys. Rev. D **86**, 034506 (2012) [arXiv:1202.4914 [hep-lat]].
25. Particle Data Group (J. Beringer *et al.*), Phys. Rev. D **86**, 010001 (2012), and online updates at <http://pdg.lbl.gov/>.

26. Heavy Flavor Averaging Group Collab. (Y. Amhis *et al.*), “Averages of B-Hadron, C-Hadron, and tau-lepton properties as of early 2012,” arXiv:1207.1158 [hep-ex]. Numerical values are from <http://www.slac.stanford.edu/xorg/hfag/semi/index.html>.
27. J. Charles, O. Deschamps, S. Descotes-Genon, R. Itoh, H. Lacker, A. Menzel, S. Monteil and V. Niess *et al.*, Phys. Rev. D **84**, 033005 (2011) [arXiv:1106.4041 [hep-ph]]. Numerical values are from the FPCP-2013 online updates at <http://ckmfitter.in2p3.fr>
28. UTfit Collab. (M. Bona *et al.*), Phys. Lett. B **687**, 61 (2010) [arXiv:0908.3470 [hep-ph]]. Numerical values are from the summer 2013 online updates at <http://www.utfit.org/UTfit/ResultsSummer2013PostEPS>
29. A. Khodjamirian, T. Mannel, N. Offen and Y. -M. Wang, Phys. Rev. D **83**, 094031 (2011) [arXiv:1103.2655 [hep-ph]].
30. A. Crivellin, Phys. Rev. D **81**, 031301 (2010) [arXiv:0907.2461 [hep-ph]].
31. A. J. Buras, K. Gemmler and G. Isidori, Nucl. Phys. B **843**, 107 (2011) [arXiv:1007.1993 [hep-ph]].
32. E. Lunghi and A. Soni, Phys. Lett. B **697**, 323 (2011) [arXiv:1010.6069 [hep-ph]].
33. S. Fajfer, J. F. Kamenik, I. Nisandzic and J. Zupan, Phys. Rev. Lett. **109**, 161801 (2012) [arXiv:1206.1872 [hep-ph]].
34. CLEO Collab. (G. Brandenburg *et al.*), Phys. Rev. D **61**, 072002 (2000) [hep-ex/9907057].
35. ARGUS Colla. (H. Albrecht *et al.*), Phys. Lett. B **255**, 297 (1991).
36. BABAR Collab. (B. Aubert *et al.*), hep-ex/0304020 (2003), Presented at 38th Rencontres de Moriond on Electroweak Interactions and Unified Theories, 15-22 Mar 2003, Les Arcs, France.
37. M. Feindt, F. Keller, M. Kreps, T. Kuhr, S. Neubauer, D. Zander and A. Zupanc, Nucl. Instrum. Meth. A **654**, 432 (2011) [arXiv:1102.3876 [hep-ex]].
38. Belle Collab. (I. Adachi *et al.*), Phys. Rev. Lett. **110**, 131801 (2013) [arXiv:1208.4678 [hep-ex]].
39. BABAR Collab. (B. Aubert *et al.*), Phys. Rev. D **76**, 052002 (2007) [arXiv:0705.1820 [hep-ex]].
40. CLEO Collab. (J. P. Alexander *et al.*), Phys. Rev. Lett. **77**, 5000 (1996).
41. A. Matyja *et al.* [Belle Collaboration], Phys. Rev. Lett. **99**, 191807 (2007) [arXiv:0706.4429 [hep-ex]].
42. Belle Collab. (A. Bozek *et al.*), Phys. Rev. D **82**, 072005 (2010) [arXiv:1005.2302 [hep-ex]].
43. Belle Collab. (I. Adachi *et al.*), arXiv:0910.4301 [hep-ex].
44. BABAR Collab. (B. Aubert *et al.*), Phys. Rev. Lett. **104** (2010) 011802 [arXiv:0904.4063 [hep-ex]].
45. BABAR Collab. (B. Aubert *et al.*), Phys. Rev. D **79**, 012002 (2009) [arXiv:0809.0828 [hep-ex]].
46. BABAR Collab. (B. Aubert *et al.*), Phys. Rev. D **77**, 032002 (2008) [arXiv:0705.4008 [hep-ex]].
47. A. Bozek, presentation at the 11th International Conference on Flavor Physics and CP Violation, Rio de Janeiro, 19-24 May, 2013.
48. ALEPH Collab. (R. Barate *et al.*), Eur. Phys. J. C **19**, 213 (2001) [hep-ex/0010022].
49. Heavy Flavor Averaging Group, [http://www.slac.stanford.edu/xorg/hfag/osc/PDG\\_2013/#FRACZ](http://www.slac.stanford.edu/xorg/hfag/osc/PDG_2013/#FRACZ).
50. ARGUS Collab. (H. Albrecht *et al.*), Phys. Lett. B **353**, 554 (1995).
51. CLEO Collab. (M. Artuso *et al.*), Phys. Rev. Lett. **75**, 785 (1995).
52. CLEO Collab. (T. E. Browder *et al.*), Phys. Rev. Lett. **86**, 2950 (2001) [hep-ex/0007057].

53. ALEPH Collab. (D. Buskulic *et al.*), Phys. Lett. B **343**, 444 (1995).
54. L3 Collab. (M. Acciarri *et al.*), Phys. Lett. B **396**, 327 (1997).
55. BABAR Collab. (B. Aubert *et al.*), Phys. Rev. Lett. **95**, 041804 (2005) [hep-ex/0407038].
56. BABAR Collab. (B. Aubert *et al.*), Phys. Rev. D **73**, 057101 (2006) [hep-ex/0507069].
57. BABAR Collab. (B. Aubert *et al.*), Phys. Rev. D **81**, 051101 (2010) [arXiv:0912.2453 [hep-ex]].
58. Belle Collab. (K. Hara *et al.*), Phys. Rev. D **82**, 071101 (2010) [arXiv:1006.4201 [hep-ex]].
59. Belle Collab. (K. Ikado *et al.*), Phys. Rev. Lett. **97**, 251802 (2006) [hep-ex/0604018].
60. BABAR Collab. (B. Aubert *et al.*), Phys. Rev. D **77**, 011107 (2008) [arXiv:0708.2260 [hep-ex]].
61. BABAR Collab. (J. P. Lees *et al.*), Phys. Rev. D **88**, 031102 (2013) [arXiv:1207.0698 [hep-ex]].
62. G. Aad *et al.* [ATLAS Collaboration], JHEP **1206**, 039 (2012) [arXiv:1204.2760 [hep-ex]].
63. S. Chatrchyan *et al.* [CMS Collaboration], JHEP **1207**, 143 (2012) [arXiv:1205.5736 [hep-ex]].
64. R. Dutta, A. Bhol and A. KGiri, Phys. Rev. D **88**, 114023 (2013) [arXiv:1307.6653 [hep-ph]].
65. P. Biancofiore, P. Colangelo and F. De Fazio, Phys. Rev. D **87**, no. 7, 074010 (2013) [arXiv:1302.1042 [hep-ph]].
66. I. Dorner, S. Fajfer, N. Konik and I. Niandi, JHEP **1311**, 084 (2013) [arXiv:1306.6493 [hep-ph]].
67. Y. Sakaki, M. Tanaka, A. Tayduganov and R. Watanabe, Phys. Rev. D **88**, 094012 (2013) [arXiv:1309.0301 [hep-ph]].
68. P. Ko, Y. Omura and C. Yu, JHEP **1303**, 151 (2013) [arXiv:1212.4607 [hep-ph]].
69. N. G. Deshpande and A. Menon, JHEP **1301**, 025 (2013) [arXiv:1208.4134 [hep-ph]].
70. A. Abada, A. M. Teixeira, A. Vicente and C. Weiland, arXiv:1311.2830 [hep-ph].
71. X. -G. He and G. Valencia, Phys. Rev. D **87**, 014014 (2013) [arXiv:1211.0348 [hep-ph]].
72. A. Celis, M. Jung, X. -Q. Li and A. Pich, JHEP **1301**, 054 (2013) [arXiv:1210.8443 [hep-ph]].
73. B. Meadows, M. Blanke, A. Stocchi, A. Drutskoy, A. Cervelli, M. Giorgi, A. Lusiani and A. Perez *et al.*, arXiv:1109.5028 [hep-ex].